

Table 3.33: Test sequence for thermal vacuum test.

Step	Phase	Description	Details
1	Phase 1	Initial checks	As needed
2		Start CAN data acquisition	
3		Pumpdown	Vacuum level: $P < 10e - 5$ bar
4		Shroud cooling down to -180°C	Auxiliary heaters on to ensure limit inoperative temperature to electronics
5		H1, H2, H3 on at $\sim 50\text{ W}$	3.12 A , $17.27\text{ V} = 53.88\text{ W}$
6		Temperature stabilization	Decrease wattage when motherboards reach 70°C (*)
7	Phase 2	H1, H2, H3 on at $\sim 30\text{ W}$	2.31 A , $12.87\text{ V} = 29.73\text{ W}$
8		Threshold command to all smart skins	Lower threshold = 68°C Upper threshold = 70°C
9		Temperature stabilization	Leave electronics at 70°C for at least 30 minutes
10		Stop LN2, start shroud heating	
11		H1 to H3 off	When shrouds have reached minimum non operative temperature for electronics
12		Stop CAN data acquisition	
13		Shroud heating up to $+20^{\circ}\text{C}$	To avoid letting TVC shrouds cold during short test break
14	Phase 3	Shroud cooling down to -180°C	If necessary, auxiliary heaters on to ensure limit inoperative temperature to electronics
15		Start CAN data acquisition	
16		H1, H2, H3 on at $\sim 8.5\text{ W}$	6.8 V , $1.24\text{ A} = 8.43\text{ W}$
17		Verify coherence of collected data (smart skin vs thermocouples)	Wait for temperature to drop to -20°C
18		Duty Cycle Command to smart skins	5% duty cycle
19		Temperature stabilization	Leave electronics at low temperature for at least 30 minutes (*)
20		H1, H2, H3 off	

Table 3.33: Test sequence for thermal vacuum test.

Step	Phase	Description	Details
21	Phase 4	Power on to all dummy units (~ 1.5 W each)	D51 // D42 = 1.95 V, 1.52 A = 2.97 W D52 // D41 = 1.95 V, 1.36 A = 2.65 W D31 // D22 = 2.62 V, 1.12 A = 2.93 W D32 // D21 = 2.45 V, 1.22 A = 2.99 W
22		Threshold command to all smart skins	Upper threshold = 20°C Lower threshold = 19°C
23		Temperature stabilization	Leave electronics at target temperature for at least 30 minutes (*)
24		Power off to all dummy units	
25	Phase 5	Power on to dummy units ("Zig-zag pattern")	D51 // D42 = 0 W D31 // D22 = 0 W D32 // D21 = 2.83 V, 1.41 A = 3.99 W D52 // D41 = 2.38 V, 1.68 A = 4.00 W
26		Threshold command to all smart skins	Upper threshold = 10°C Lower threshold = 9°C
27		Temperature stabilization	Leave electronics at target temperature for at least 30 minutes (*)
28		Stop LN2, start shroud heating	
29		Dummy units off	If necessary, auxiliary heaters H1 to H3 on to ensure limit inoperative temperature to electronics
30		H1, H2, H3 off	When shrouds have reached minimum non operative temperature for electronics
31		Stop CAN data acquisition	
32		Shroud heating up to +20°C	To avoid letting TVC shrouds cold during short test break
33	Phase 6	Shroud cooling down to -180°C	If necessary, auxiliary heaters on to ensure limit inoperative temperature to electronics
34		Start CAN data acquisition	

Table 3.33: Test sequence for thermal vacuum test.

Step	Phase	Description	Details
35		Power on to dummy units D32 and D21	D32 // D21 = 2.85 V, 1.41 A = 4.02 W
36		Smart skins: all heaters on	300 mW for each heater
37		Smart skins: all heaters on	800 mW for each heater
38		D51+D42 and D31+D22 on D32+D21 off	10W on each active couple: D51 // D42 = 3.60 V, 2.80 A = 10.08 W D31 // D22 = 4.72 V, 2.07 A = 9.77 W D32 // D21 = 0 W D52 // D41 = 0 W
39		Threshold command to all smart skins	Lower threshold = 68°C Upper threshold = 70°C
40		Temperature stabilization	Leave electronics at target temperature for at least 30 minutes (*)
41		Stop CAN data acquisition	
42	Phase 7	Shroud cooling off	If necessary, auxiliary heaters H1 to H3 on to ensure limit inoperative temperature to electronics
43		Pressure recovery (to ambient)	
44		Power switch off	
45		Final checks	As needed

(*) Since thermal balance is not stringent, usual stabilization criterion ($\Delta T < 0.5$ °C/hr, measured near the powered heaters) does NOT apply.

Table 3.34: Temperature limits for Smart Skin electronics.

Component	Description	Inoperative range		Operative Range	
		T Min [°C]	T Max [°C]	T Min [°C]	T Max [°C]
D ES3J SMC	Ultra fast diode	-55	150	-55	150
TR SI2309CDS SOT23 VSH	Mosfet	-55	150	-55	150
TR SI2308BDS-T1-GE3 SOT23 VSH	Mosfet	-55	150	-55	150
IC LM5010SD LLP10 NAT	Buck regulator	-55	150	-40	125
IC MCP2551-E/SN SO8 MCP	CAN transceiver	-55	150	-40	125
IC TMP175 SO8	Temp. sensor	-60	130	-55	127
IC MCP9803-M/SN SO8	Temp. sensor	-65	150	-55	125
IC ADXL321JCP LFCSP16	Accelerom.	-65	150	-20	70
IC PIC18F2580-I/SO SO28W	Micro	-65	150	-40	125
IC LMC6482AIM/NOPB SO8	Rail-To-Rail Input and Output Operational Amplifier	-65	150	-55	125
IC MCP23008-E/SO SO18W	I/O expander	-65	150	-40	125
IC MAX232IDW SO16	232 IF	-65	150	-40	85
Capacitors		(all except those mentioned hereinafter)			
CEL 10UF 50V 20% 6,3X5,3 SMD		Capacitore			
Resistors		(all except those mentioned hereinafter)			
CCR 5R6 5% 1W 2512		Resistor			
R 75R 20% 100X30		Heater			

Table 3.34: Temperature limits for Smart Skin electronics.

Component	Description	Inoperative range		Operative Range	
		T Min [°C]	T Max [°C]	T Min [°C]	T Max [°C]
IND 220uH LPS3010-224MLC 3.0 X 3.0 SMD	Inductor	-40	125	-40	85
DIP SWITCH 6V A6S-6102-H DIL12 OMRON	Switch	n.d.	n.d.	-20	70
CONN TMM-112-01-G-S-SM SAM P2.0 SMD	Connectors	n.d.	n.d.	-55	125
INVILUPPO		-40	125	-20	70

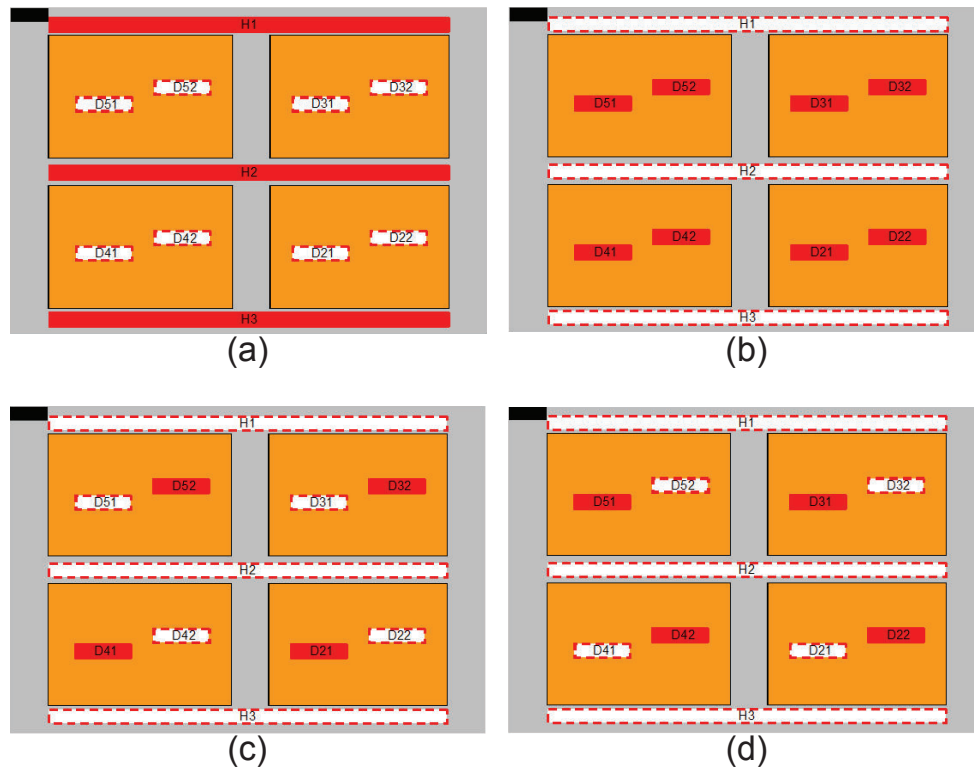


Figure 3.55: Thermal vacuum test: load layout for cases 1 and 2 (a), 3 (b), 4 (c), and 5 (d).

Ambient test generalities

The purpose of the test is to verify the possibility to use a Smart Skin - like layer in deployable structures and therefore to check mechanical and thermal behavior of flexible PI/Cu circuitry when bonded to Kevlar fabric. The test prepared for SDC is intended as a functional room-condition bench test.

The ambient test is carried out in the Thermal Systems Engineering Technological Area (TS-ETA), at Thales Alenia Space premises. The facility offers a fluid servicer and a small vacuum chamber. In the same area were performed also all other test-related activities (hardware-software integration, bench testing, troubleshooting...).

Ambient test set-up and instrumentation

The SDC test article is instrumented with a suitable number of temperature sensors (thermocouples):

- 4 TCs on the demonstrator +z skin (electronic side).
- 4 TCs on the demonstrator -z skin (back side).

Figure 3.56 show position and numbering of the 8 SDC thermocouples.

All thermocouples are acquired via an analogue-to-digital interface, which is easily connected to the control workstation via a USB port. For this reason, in

Table 3.35: Thermal vacuum test cases.

Case 1	
Case 1 refers to Phase 2 of Table 3.33. Total power summing up to 30 W.	heater H1 = 10 W heater H2 = 10 W heater H3 = 10 W
Case 2	
Case 2 refers to Phase 3 of Table 3.33. Total power summing up to 8.5 W.	heater H1 = 2.8 W heater H2 = 2.8 W heater H3 = 2.8 W
Case 3	
Case 3 refers to Phase 4 of Table 3.33. Total power summing up to 8.5 W.	heater D21 = 1.5 W heater D22 = 1.5 W heater D31 = 1.5 W heater D32 = 1.5 W heater D41 = 1.5 W heater D42 = 1.5 W heater D51 = 1.5 W heater D52 = 1.5 W
Case 4	
Case 4 refers to Phase 5 of Table 3.33. Total power summing up to 8 W.	heater D41 = 2 W heater D52 = 2 W heater D21 = 2 W heater D32 = 2 W
Case 5	
Case 5 refers to Phase 6 of Table 3.33. Total power summing up to 20 W.	heater D51 = 5 W heater D42 = 5 W heater D31 = 5 W heater D32 = 5 W

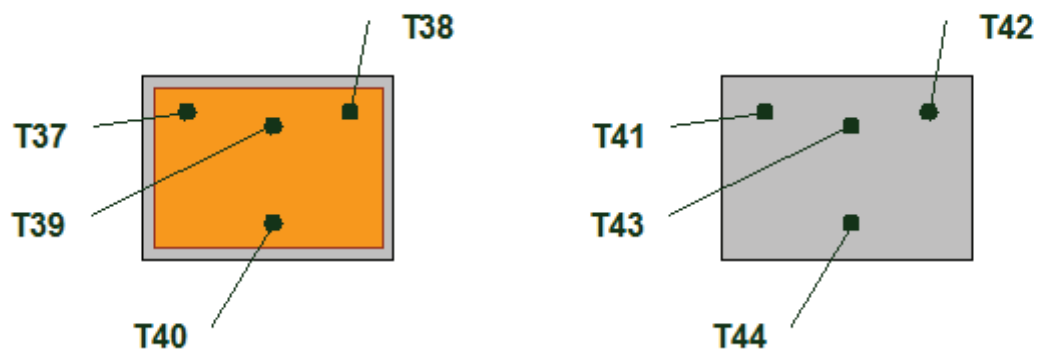


Figure 3.56: Thermocouples aboard SDB.

Table 3.36: Description of TC pairs.

Front	Rear	Description of location
Channel 1 (T37)	Channel 5 (T41)	Between sensors U14 and U19
Channel 2 (T38)	Channel 6 (T42)	Between sensors U16 and U23
Channel 3 (T39)	Channel 7 (T43)	Between U28 and U30 (microcontroller and I/O expander)
Channel 4 (T40)	Channel 8 (T44)	Near U27 (accelerometer)

the test results, the eight thermocouples are labelled as Channel 1 to Channel 8 (respectively, T37 to T44). The sensors are coupled as reported in Table 3.36.

This demonstrator hosts a network made of 17 direct-to-digital temperature sensors and is connected via CAN bus to a PC / user interface for data acquisition and heater control.

Contrary to what was done with SDA and SDB, STEPS Demonstrator C has no tape heater segments serving as dummy units.

Additional equipment needed to carry out the test is:

- 1 DC power unit (maximum power ~ 200 W), in order to feed the motherboard.
- 1 data acquisition system for thermocouples.
- 1 CAN-USB interface required in order to read CAN data.
- One PC, in order to gather and show data from MBs and thermocouples.

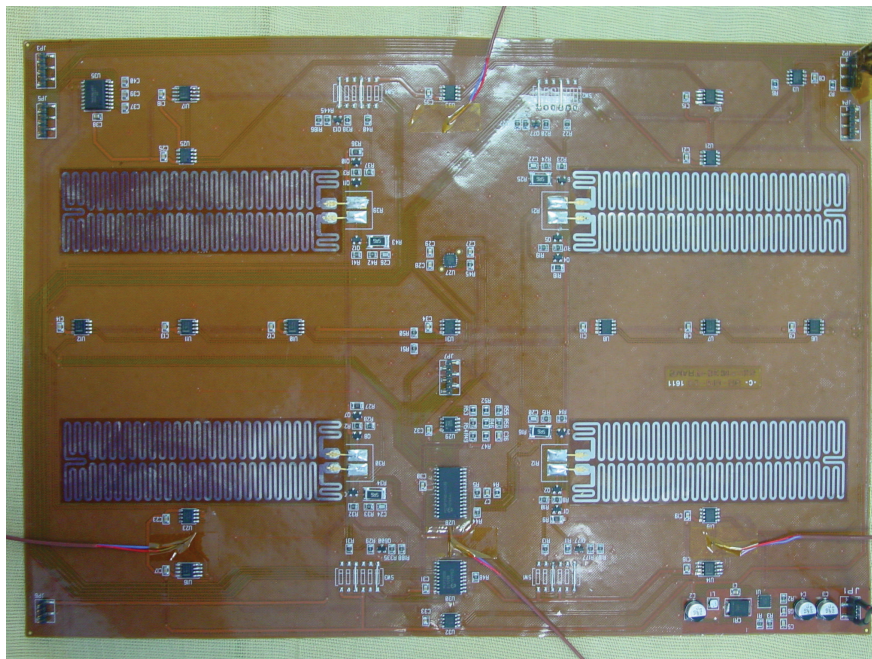


Figure 3.57: Instrumented upper face of the SDC prototype (+z side).

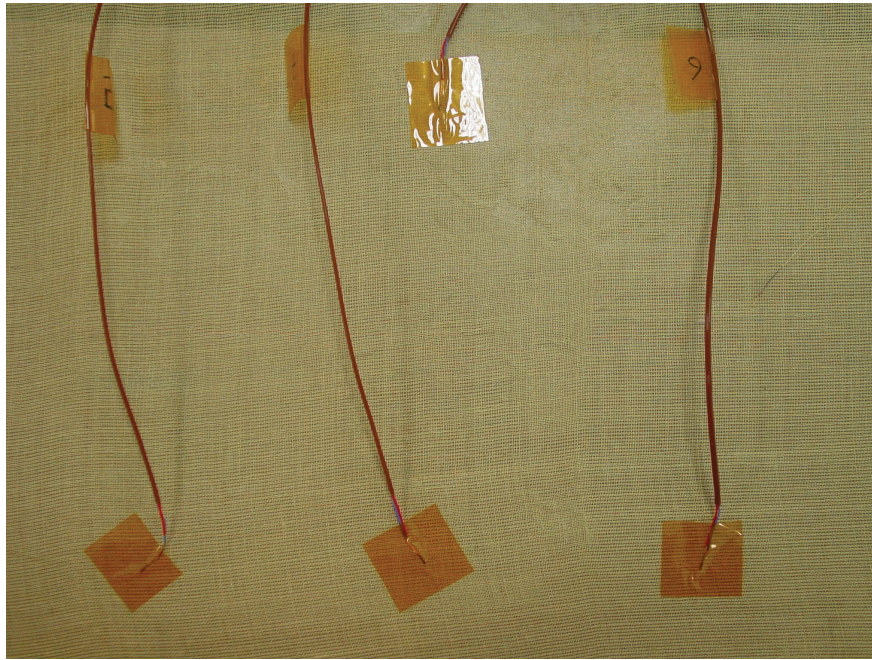


Figure 3.58: Instrumented lower face of the SDC prototype (-z side).

The ambient test prototype is connected to power and signal by means of connections built for the thermal vacuum test (SDA and SDB).

Ambient test approach

The test article is located on an insulating baseplate on the test bench in the Thermal Control Technological Area (Figure 3.59). The test consists of a functional (thermal control) test under room conditions. Test environment conditions are:

- Pressure: $P = 996 \text{ mbar}$ (0.98 atm).
- Temperature: $T = 20 \div 23 \text{ }^{\circ}\text{C}$.
- Upper face (+z side) of the panels (mounting electronics) exposed to ambient, free.
- Lower face (-z side) in contact with supporting baseplate.

Temperature data from the integrated electronics and from auxiliary sensors are acquired for the whole duration of the test with a suitable scan rate (minor or equal to $\Delta t = 60 \text{ s}$ for thermocouples, $\Delta t = 5 \text{ s}$ for digital sensors).

During test activities, various plateaus are carried out, characterized by different control laws, according to the test sequence described in Table 11.

During test, scrupulous attention is paid to COTS electronics requirements, in particular, to limit temperatures. Consult aforementioned Table 3.34 for details.

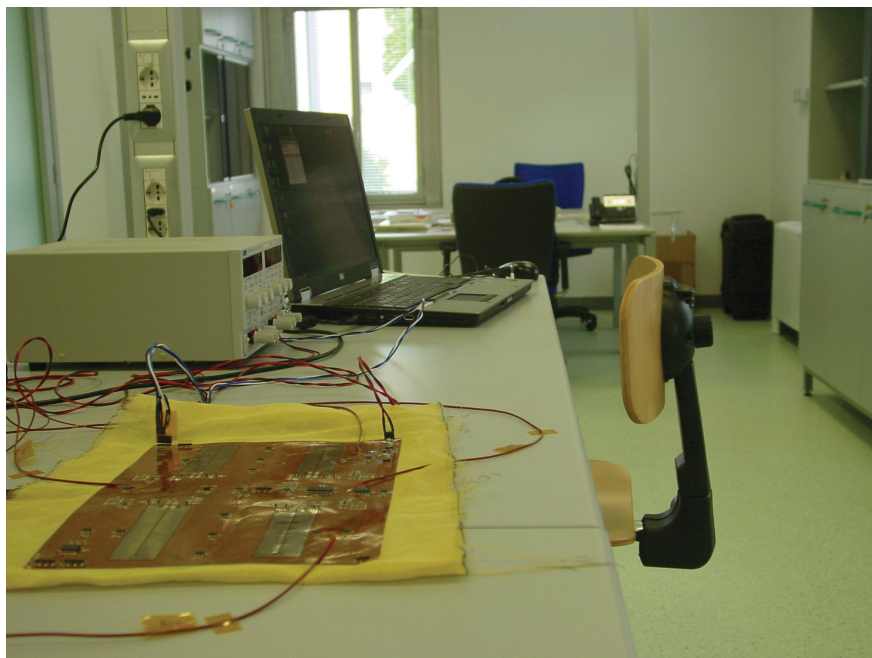


Figure 3.59: SDC assembly ready for test.

Table 3.37: Test sequence for ambient test.

Step	Phase	Description	Details
1	Phase 1	Initial checks	As needed
2		Note ambient pressure	Pamb = 1007 mbar
3		Note ambient temperature	Tamb = 23.3 °C
4		Start CAN data acquisition	
5		Verify coherence of collected data (smart skin vs thermocouples)	Check readings over a 15 minutes period
6	Phase 2	Note ambient pressure	Pamb = 998 mbar
7		Note ambient temperature	Tamb = 20.3 °C
8		Command smart skin to keep temperature at Tamb + 5°C	
9		Run “temperature threshold” control law	Leave electronics working for 30 minutes (*)
10	Phase 3	Command smart skin to dissipate 1W on each heater	Given target is an average value obtained through PWM
11		Run “power target” control law	Leave electronics working for 30 minutes (*)
12	Phase 4	Note ambient pressure	Pamb = 996 mbar
13		Note ambient temperature	Tamb = 21.6 °C
14		Command smart skin to increase heater temperature by 1°C/s	
15		Run “temperature gradient target” function	Leave electronics working for 30 minutes (*)
16	Phase 5	Command smart skin to keep all heaters at 20% duty cycle.	
17		Run “command duty cycle” function	Leave electronics working for 30 minutes (*)

Table 3.37: Test sequence for ambient test.

Step	Phase	Description	Details
18	Phase 6	Command smart skin to keep temperature at 70°C	
19		Run “temperature threshold” control law	Leave electronics working for 30 minutes (*)
20	Phase 7	SDC cooling off	To Tamb = 20.0 °C
21		Command smart skin to keep temperature at Tamb + 5°C	
22		Manually flex and move SDC	
23		Verify coherence of temperature data (smart skin vs TCs) and accelerometer data	
24	Phase 8	Power switch off	
25		SDC cooling off	To Tamb
26		Final checks	As needed
(*) Since thermal balance is not stringent, usual stabilization criterion ($\Delta T < 0.5\text{ °C/hr}$, measured near the powered heaters) does NOT apply.			

3.2.3 JPL μ Rover

After the design of the JPL μ Rover was complete, two mock-ups were built, to test the following aspects:

- Full electrical functionality of the architecture (with identification of possible design defects).
- Viability of the geometrical layout, and evaluation of integration issues.
- Behavior of the rover's control software and algorithms, including the graphical user interface.

The two photographs in Figure 3.60 show the first mock-up, whose structural elements have been built via stereolithography and are made of ABS plastic. As can be easily noticed, the chassis is overcrowded with all the electronics and harness needed to make the rover work. The advantages of using a MFS approach can be immediately appreciated if these photos are compared with the digital mock-up depicted in Figure 3.61, that shows the final configuration for the μ Rover.

This first mock-up has been exploited first of all to identify potential corrections in the geometry.

There were no mayor defects in the design of the components. Only two details were slightly modified: the first was the size of the cutouts in the port and starboard panels of the main body. Since, according to the final design, the motors are inside the rover while wheels are mounted outside the chassis, the rectangular cutouts are needed to host the servos' shafts. A slightly larger size helps with the correct positioning of the servomotors (whose front side is not flat) against the lateral panels. The second detail was the size of the central alignment hole of each wheel. In the beginning, this hole was thought just as a reference mark during the bonding of the wheels to the servos' horns. Once the bonding was in place, it was impossible to remove the wheel from the horn and the wheel-horn subassembly from the servo, because the wheel's disc itself buried the axial screw that fastened the horn to the motor. This condition did not hamper the functionality of the system, but having the possibility to remove the wheels from the motors was a characteristic that could improve ease of integration and maintenance. Slightly widening the central alignment holes allowed permanent access to the fastening screw, therefore enabling mounting and demounting of the wheels from the motors (however, wheels and horns cannot be detached from each other).

Another aspect that has been evaluated with the first prototype was the feasibility of the configuration. The distribution of the units foreseen in the digital mock-up was based on CAD models created from data obtained from datasheets; therefore, changes in the layout and dimensions were foreseen after the integration of the real components. However, all the COTS items matched exactly with their digital models, therefore no change was needed and the configuration was confirmed. This check was particularly relevant for the robotic arm, where modifications in the design would have implied correction of the kinematic models.

In second instance, the same prototype was used as a test bench for software development. The first objective was to keep the command-actuation delay as short as possible. The first tests with the 3D model showed that the software was light



Figure 3.60: JPL μ Rover: top view (left) and side view (right) of the first mock-up. Top panel has been removed to show the crowded chassis.

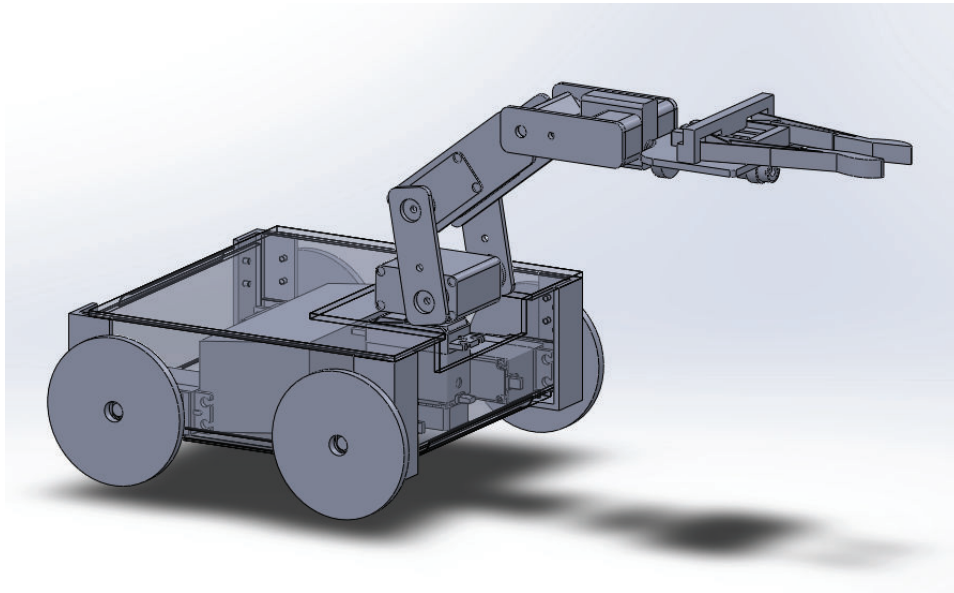


Figure 3.61: Rover 3D model showing all the main components.

enough and the encoding overhead in the communication protocol was minimal: there was no sensible delay between command and actuation. A second result was the software correction of servos' ranges. Each motor is piloted through a Pulse Width Modulation (PWM) signal, which is interpreted by the servo's onboard controller. The pulse width is usually prescribed by the datasheet in such a way to always keep the motor operating in a safe mechanical range. However, it is possible to expand the PWM range and push the servo nearer to its physical limitations. In this case, all motors were tested in their extended range, and new SW limitations on the control PWM signal were introduced to avoid jitter or hitting of mechanical stops.

The graphical user interface (see Figure 3.64) and the control software for the robotic arm underwent extensive testing. Minor graphical formatting defects were corrected in the GUI, namely addition of a section including status messages, to allow an easier understanding of the reasons for rejected user input, and updating of the graphs displaying the rover configuration, that have been subordinated to the successful generation of a feasible joint set, so that no blank figure is shown in case the user request is badly formatted or asking for a solution out of the rover's workspace.

The second mock-up (see Figure 3.63) was used to perform a final functional test of the whole system. This included evaluation of the geometrical design, evaluation of the electrical design, evaluation of the software, and evaluation of the graphical user interface.

Under a mechanical point of view, after the corrections coming from the testing of the first prototype, no problems were encountered. The rigid-flex PCB body of the rover integrated smoothly with the 3D-printed spacers and with the COTS components. It proved the capability of the PCB manufacturing process to build a component with sufficient dimensional accuracy to be integrated as a structural member.

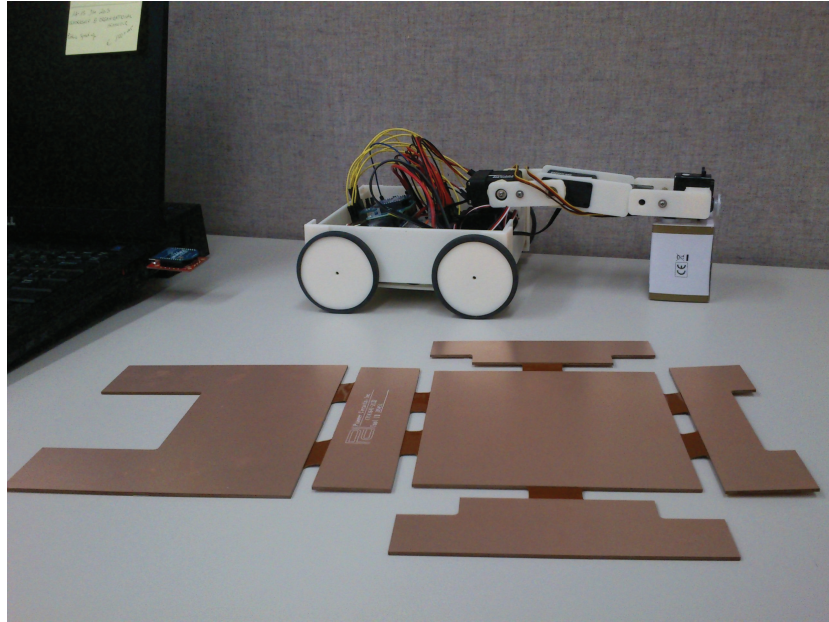


Figure 3.62: JPL μ Rover: first mock-up and unfolded body of the second mock-up.

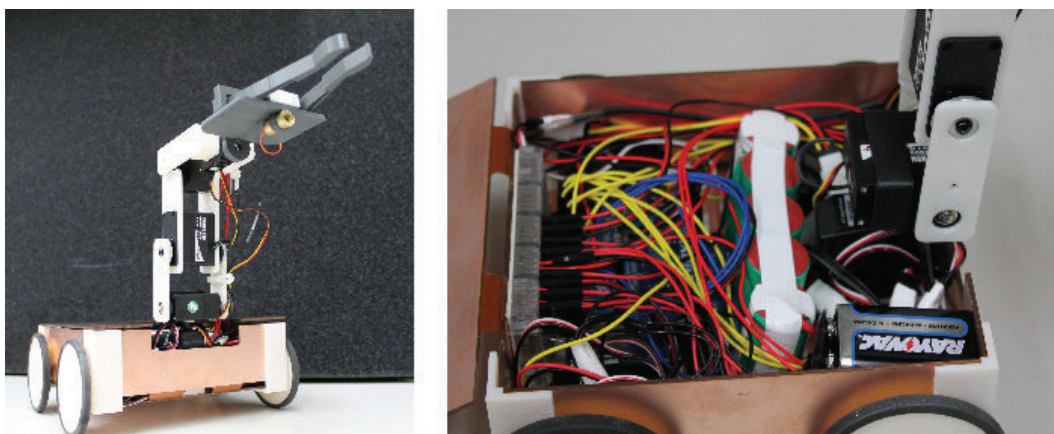


Figure 3.63: JPL μ Rover: overall view (left) and body view (right) of the second mock-up.

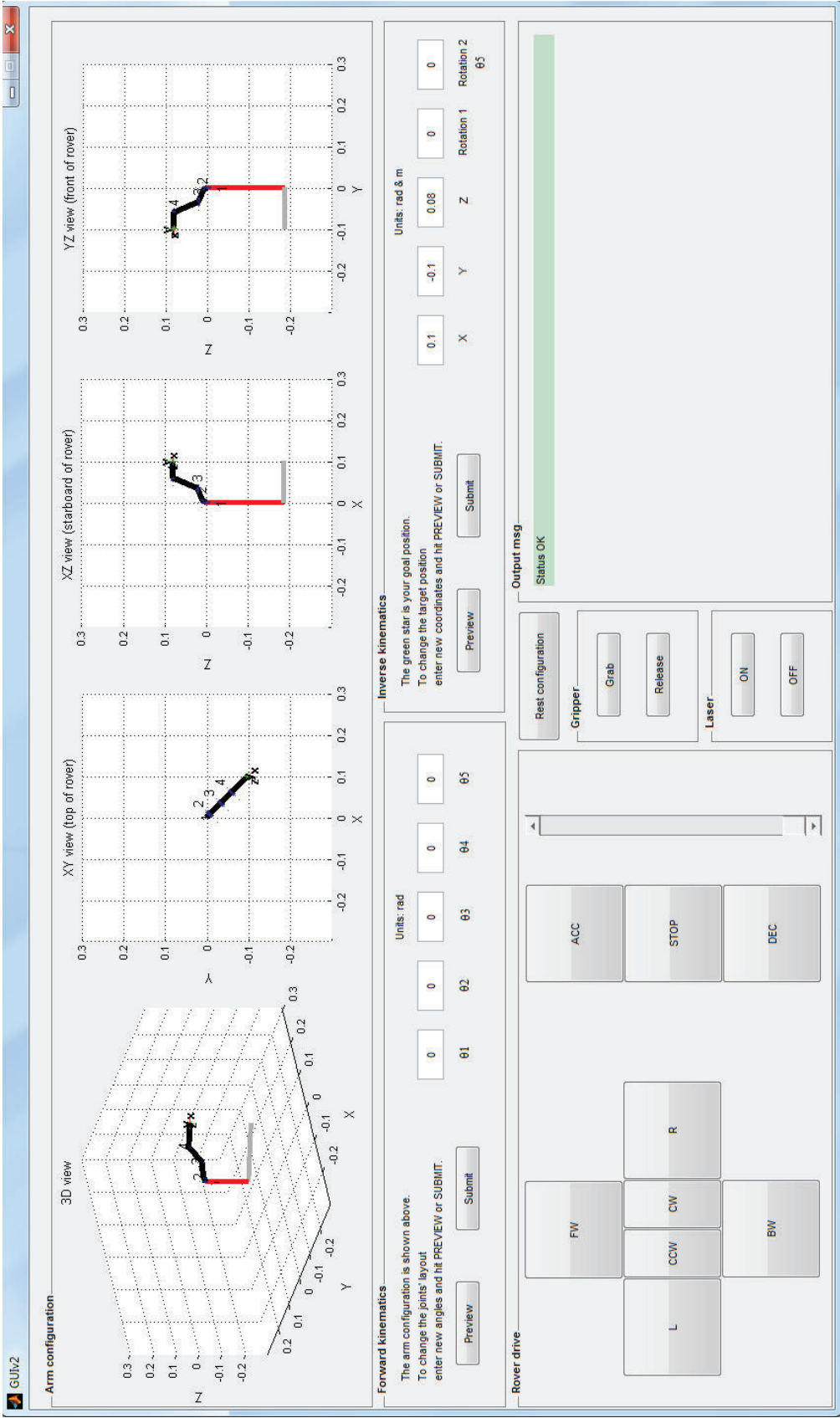


Figure 3.64: A screenshot of the Graphical User Interface for the JPL μ Rover.

The electrical design proved to be correct and effective. The rover operated according to its specifications, with all the foreseen functions.

The software was adequate for a small agile system. The code running on the onboard microcontroller was light and reliable. It executed quickly and flawlessly even within the memory and computational power limitations of the ATMEGA microcontroller. The software running on the control station, on the other hand, was complex and flexible enough to handle high-level functions. The routines written to control the kinematics of the arm were fast and dependable, mainly thanks to the closed analytical form of the solution. In fact, as a matter of comparison, an iterative algorithm included in the Matlab Robotics Toolbox [81] was also tested, and it resulted in slower code execution and impossibility to spot alternate configurations.

The graphical user interface was handy and intuitive, and allowed a quite easy control of the vehicle. Two possible improvements were pointed out after the test campaign. The first is the introduction of a filter function on user input, to reject or correct misformatted and inadmissible values. Up to now, check functions only evaluate the feasibility of the input, assuming that it is entered with a proper syntax. A more thorough control of the user input would make the GUI more reliable.

The second improvement is the inclusion of a data acquisition (DAQ) system based on a midi joystick peripheral, that would make the guidance of the rover even more intuitive.

Chapter 4

Lesson Learned and Results

Analysis and Discussion

4.1 ABB

Under a structural point of view, the first mechanical tests after manufacturing evidenced that the connection between skins and honeycomb was neither uniform nor reliable. The highlighted problem had already been observed in severe form during manufacturing of preliminary breadboards: the bonding process was not properly developed and verified. The impact of the aforementioned inaccuracies on the panel performance is not yet clear. The evaluation of the results and the observations made during the mechanical tests on the C/C sandwich panel led to the following conclusions:

- The tensile Young's modulus of the quasi-isotropic facings was close to the value expected on the basis of the composite architecture, the fiber's properties (declared by manufacturer), and the fiber content.
- The facings' strength proved to be definitely low, probably because the material had a heterogeneous microstructure (fibers, matrix and large voids/cracks) that was heavily affected by the processing route.
- The sandwich specimens, whatever the test performed (tension or flexure), showed a recurring failure mode at the honeycomb/facing interface, associated to very low failure loads.
- The graphitized adhesive (SGL Group) had poor adhesion to both the honeycomb and the facings and turned out to be the real weak link of the structure.
- Sandwich structures made of fibers and materials used for ABB might be suitable for lightly loaded high-stability components (e.g. payload supports), but appear inappropriate for primary structural applications.

In the beginning, a troubleshooting activity was initiated in collaboration with the manufacturer, with the intent of tuning the high temperature graphitization process and improving the reliability of C/C junction. However, the initiative did

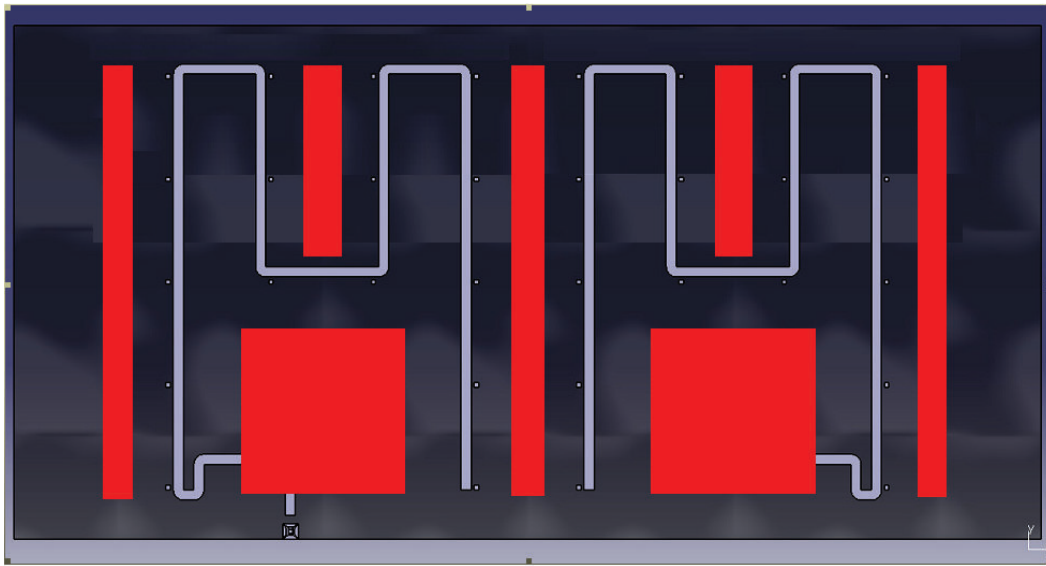


Figure 4.1: ABB test case 1.

not work, and all the aforementioned considerations led to the decision of setting aside the work on innovative Carbon-Carbon materials, and focus instead on the development of a product that could add multifunctionality to whatever support structure the designer would choose. In this way, ABB was the catalyst of the smart skin concept.

Under a thermal point of view, the main purposes of the test were:

- To estimate the thermal performance of the panel in terms of heat rejection capability in different power dissipation configurations.
- To verify the behavior of COTS electronics in a thermal-vacuum environment representative of space applications.
- To verify mechanical and thermal behavior of flexible PI/Cu circuitry.

The ABB thermal vacuum test was composed of five cases.

- Case 1 refers to Phase 2 of Table 3.28. Total power was summing up to 125 W (see Figure 4.1):
 - H1, H3, H5 at 25 W.
 - H2, H4 at 12.5 W.
 - MB left, MB right at 12.5 W.
- Case 2 refers to Phase 3 of Table 3.28. Total power was summing up to 190 W (see Figure 4.2):
 - H1, H3, H5 at 50 W.
 - H2, H4 at 20 W.



Figure 4.2: ABB test case 2.

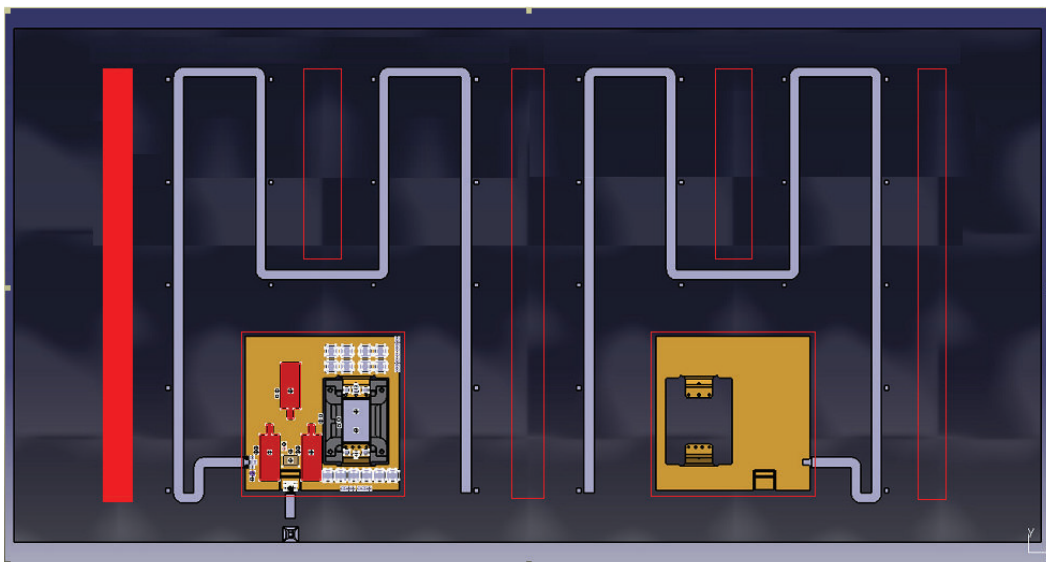


Figure 4.3: ABB test case 3.

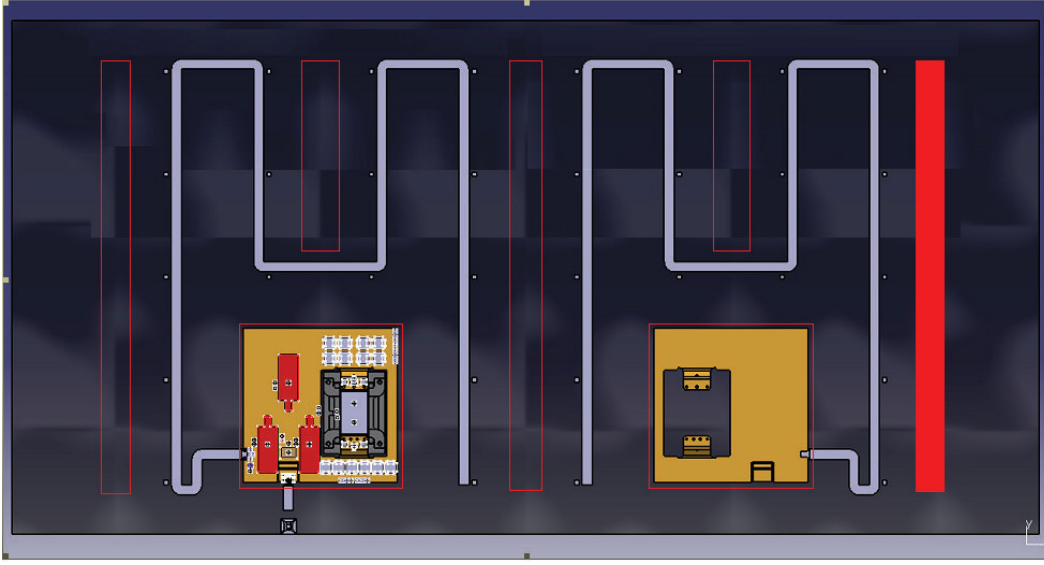


Figure 4.4: ABB test case 4.

- Case 3 refers to Phase 4 of Table 3.28. Total power was summing up to 100 W (see Figure 4.3): H1 at 100 W.
- Case 4 refers to Phase 5 of Table 3.28. Total power was summing up to 100 W (see Figure 4.4): H5 at 100 W.
- Case 5 refers to Phase 6 of Table 3.28. Total power was summing up to 80 W (see Figure 4.1):
 - H1 at 50 W.
 - MB right at 30 W.

After the computation of corrected radiative couplings (GR), obtained from a Geometrical Mathematical Model (GMM) with an emissivity value of $\varepsilon = 0.43$ (measured, and opposed to an anticipated $\varepsilon = 0.8$), the correlation of the Thermal Mathematical Model (TMM) allowed to give a better estimate of the thermal conductivity of the panel in the three spatial direction. The conductivity in the skin-to-skin direction (k_z) was obtained by working with the test case characterized by a uniform power distribution (Case 1), and considering the average skin temperature in steady state conditions $T_{avg -z} = 37.61 \text{ deg } C$ and $T_{avg +z} = 42.12 \text{ deg } C$ (in fact, during Case 1, with a uniform heat load distribution, it is reasonable to assume a quite uniform final temperature distribution on the plane, and therefore average temperatures are a good indicator).

On the other hand, conductivities in the planar directions can be evaluated with an asymmetric heat load distribution, like that pertaining to Case 3, where the left side of the panel is warm and the right side is quite cold. In this case, local temperatures will be considered instead of averages. Moreover, k_x and k_y are supposed equal, because the material is considered isotropic.

With the traditional manual correlation, the values that gave the best fit were those listed in Table 4.1.



Figure 4.5: ABB test case 5.

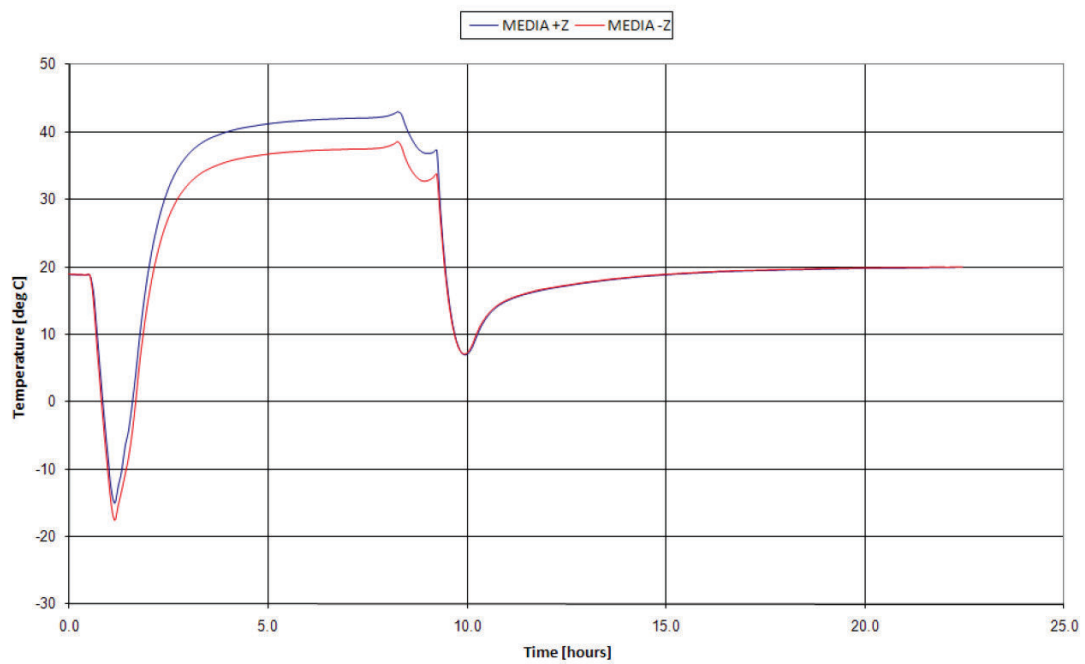


Figure 4.6: Temperatures during ABB test case 1.

Table 4.1: ABB C/C panel conductivity values (classical TMM correlation).

k_z	1.5 W/m/K
$k_x = k_y$	40W/m/K
$T_{avg -z}$	38.6°C
$T_{avg +z}$	42.15°C
Local T deviation	1°C